



DIGITAL ACCESS TO SCHOLARSHIP AT HARVARD

An Emerging Picture of Neoproterozoic Ocean Chemistry: Insights from the Chuar Group, Grand Canyon, USA

The Harvard community has made this article openly available. [Please share](#) how this access benefits you. Your story matters.

Citation	Johnston, David T., Simon W. Poulton, Carol Dehler, Susannah Porter, Jon Husson, Donald E. Canfield, and Andrew H. Knoll. An emerging picture of Neoproterozoic ocean chemistry: Insights from the Chuar Group, Grand Canyon, USA. <i>Earth and Planetary Science Letters</i> 290(1-2): 64-73.
Published Version	doi:10.1016/j.epsl.2009.11.059
Accessed	April 17, 2018 3:34:31 PM EDT
Citable Link	http://nrs.harvard.edu/urn-3:HUL.InstRepos:10059265
Terms of Use	This article was downloaded from Harvard University's DASH repository, and is made available under the terms and conditions applicable to Open Access Policy Articles, as set forth at http://nrs.harvard.edu/urn-3:HUL.InstRepos:dash.current.terms-of-use#OAP

(Article begins on next page)

1 **An emerging picture of Neoproterozoic ocean chemistry: Insights from the Chuar Group,**
2 **Grand Canyon, USA**

3
4 David T. Johnston^{a,b}, Simon W. Poulton^c, Carol Dehler^d, Susannah Porter^e, Jon Husson^a, Donald
5 E. Canfield^f, Andrew H. Knoll^b

6
7 ^aDept. of Earth and Planetary Sciences, Harvard University, 20 Oxford Street, Cambridge, MA 02138 USA

8 ^bDept. of Organismic and Evolutionary Biology, Harvard University, 26 Oxford Street, Cambridge, MA 02138 USA

9 ^cDept. of Civil Engineering and Geosciences, Newcastle University, Drummond Building, Newcastle upon Tyne,
10 NE1 7RU, UK

11 ^dDept. of Geology, Utah State University, 4505 Old Main Hill, Logan, UT 84322 USA.

12 ^eDept. of Earth Science, UC Santa Barbara, Webb Hall, Bldg 526, Santa Barbara, CA USA

13 ^fNordCEE and Institute of Biology, University of Southern Denmark, Campusvej 55, 5230 Odense M, DK.

14
15 Corresponding author is D.T. Johnston. Email: johnston@eps.harvard.edu

16 Phone: 617-496-5024 Fax: 617-495-8839

17
18
19 **Abstract:** Detailed iron, sulfur and carbon chemistry through the >742 million year old Chuar
20 Group reveals a marine basin dominated by anoxic and ferrous iron-rich (ferruginous) bottom
21 waters punctuated, late in the basin's development, by an intrusion of sulfide-rich (euxinic)
22 conditions. The observation that anoxia occurred frequently in even the shallowest of Chuar
23 environments (10s of meters or less) suggests that global atmospheric oxygen levels were
24 significantly lower than today. In contrast, the transition from ferruginous to euxinic subsurface
25 water is interpreted to reflect basinal control – specifically, increased export of organic carbon
26 from surface waters. Low fluxes of organic carbon into subsurface water masses should have
27 been insufficient to deplete oxygen via aerobic respiration, resulting in an oxic oxygen minimum
28 zone (OMZ). Where iron was available, larger organic carbon fluxes should have depleted
29 oxygen and facilitated anaerobic respiration using ferric iron as the oxidant, with iron carbonate
30 as the expected mineralogical signature in basinal shale. Even higher organic fluxes would, in
31 turn, have depleted ferric iron and up-regulated anaerobic respiration by sulfate reduction,
32 reflected in high pyrite abundances. Observations from the Chuar Group are consistent with
33 these hypotheses, and gain further support from pyrite and sulfate sulfur isotope abundances. In

34 general, Chuar data support the hypothesis that ferruginous subsurface waters returned to the
35 oceans, replacing euxinia, well before the Ediacaran emergence of persistently oxygenated
36 conditions, and even predating the Sturtian glaciation. Moreover, our data suggest that the
37 reprise of ferruginous water masses may relate to widespread rifting during the break-up of
38 Rodinia. This environmental transition, in turn, correlates with both microfossil and biomarker
39 evidence for an expanding eukaryotic presence in the oceans, suggesting a physiologically
40 mediated link among tectonics, environmental chemistry and life in the dynamic Neoproterozoic
41 Earth system.

42

43 Keywords: Neoproterozoic, oxygenation, iron, sulfur, ocean chemistry, paleobiology

44

45 **1.0. Introduction**

46 An intimate relationship exists between the chemistry of Earth's oceans and the
47 complexity and diversity of its inhabitants (e.g., Cloud, 1976; Knoll, 1992; Anbar and Knoll,
48 2002). For much of Earth history, water masses beneath the surface mixed layer were
49 predominantly anoxic, with ferruginous (anoxic and containing dissolved ferrous iron, Fe^{2+})
50 Archean seas (e.g., Holland, 1984; Walker and Brimblecombe, 1985; Isley and Abbott, 1999;
51 Farquhar et al., 2000) giving way, after 1.9-1.8 Ga, to oceans that were oxic in the surface mixed
52 layer but commonly sulfidic in subjacent water masses (Canfield, 1998; Shen et al., 2002; 2003;
53 Poulton et al., 2004a). More persistently oxic subsurface waters appeared during the latest
54 Proterozoic Ediacaran Period (Fike et al., 2006; Canfield et al., 2007; Shen et al., 2008), but
55 recent evidence suggests that this Neoproterozoic environmental transition may have been more
56 protracted and complex. Specifically, Canfield et al. (2008) presented evidence for a return to
57 ferruginous subsurface waters more than 100 million years before terminal Proterozoic oxygen
58 enrichment (Canfield et al., 2008). If ferruginous conditions were a common feature of later
59 Neoproterozoic oceans, this would have important implications for our thinking about both life
60 and biogeochemical cycling during that critical time.

61 The chemical profiles of ancient oceans reflect the interplay of oxygen (O), iron (Fe) and
62 sulfur (S) as they participate in the carbon (C) cycle. A means of testing and extending the
63 Canfield et al. (2008) hypothesis is through additional Fe-speciation chemistry (cf. Nagy et al.
64 2009), and further joining these data with complementary biogeochemical information. To

65 maximize interpretational value, however, analyses should be carried out within a well-
66 characterized stratigraphic framework, and preferably one with direct radiometric age constraints
67 and a rich fossil record (both morphological and molecular). The ~740-800 million year old
68 (Ma) Chuar Group, exposed within the Grand Canyon, Arizona, exhibits all of these attributes.
69 A well-constrained U-Pb date of 742 +/-6 Ma for volcanic ash near the top of the succession
70 (Karlstrom et al., 2000), detailed information on stratigraphy and sedimentology (Dehler et al.,
71 2001), carbon isotope chemostratigraphy (Dehler et al., 2005), organic geochemistry (Summons
72 et al., 1988; Ventura et al., 2005), and diverse microfossils (Schopf et al., 1973; Vidal and Ford,
73 1985; Porter and Knoll, 2000; Porter et al., 2003; Nagy et al., 2009) collectively provide an
74 appropriate framework for continued studies of Neoproterozoic, and particularly Chuar Group,
75 seawater chemistry. In this study, we present geochemical data that enable us to reconstruct
76 water column chemistry in the Chuar basin and use these to address three principal questions: a)
77 What combination of global and basinal conditions underpin observed chemical variations within
78 the Chuar succession? b) How do Chuar data constrain hypotheses about ferruginous water
79 masses in Neoproterozoic oceans? And c) What are the consequences of the reconstructed Chuar
80 water column for life within the Chuar basin and beyond?

81

82 **2.0 Geologic Setting**

83 The Neoproterozoic Chuar Group is part of the Grand Canyon Supergroup; it is underlain
84 by the Mesoproterozoic Unkar Group and early Neoproterozoic Nankowep Formation and
85 overlain by the mid- to late Neoproterozoic Sixtymile Formation or Cambrian strata (Fig. 1).
86 The Chuar Group is exposed exclusively in eastern Grand Canyon and includes the Galeros
87 Formation (Tanner, Jupiter, Carbon Canyon and Duppa members) and overlying Kwagunt
88 Formation, which, in turn, is subdivided into the Carbon Butte, Awatubi, and Walcott members
89 (Figs. 1 and 2; Ford and Breed, 1973). In total, the Chuar Group includes ~1600 meters of
90 gently folded, shale, with meter-scale interbeds of carbonate and sandstone (Ford and Breed,
91 1973). Facies analysis and stratigraphy suggest a wave- and tide-influenced depositional system
92 within an intracratonic basin (Dehler et al., 2001). The dolomite and sandstone beds cap meter-
93 scale cycles that reflect low to moderate amplitude sea-level changes considered to be
94 glacioeustatic in origin (Dehler et al., 2001). In combination, sedimentology and
95 cyclostratigraphy suggest that water depths fluctuated but never exceeded 10s to 100s of meters

96 throughout the interval recorded by Chuar deposition (Dehler et al., 2001). Several lines of
97 evidence, including sedimentary structures (Dehler et al., 2001), microfossils (Vidal and Ford,
98 1986; Porter and Knoll, 2000), cyclostratigraphy (Dehler et al., 2001), and geochemical records
99 (Dehler et al., 2005), suggest that the Chuar basin was in communication with the global ocean.
100 Chuar strata record deposition in an intracratonic extensional basin that formed in response to
101 the early break-up of Rodinia (Timmons et al., 2001), and is broadly similar to intracratonic and
102 rift basins seen globally at this time (Knoll et al., 1986; Rainbird et al., 1996; Dalziel, 1997;
103 Preiss, 2000; Li et al., 2003). Paleomagnetic data place the Chuar basin in the tropics, between
104 2°S and 18°N (Weil et al., 2004).

105 The age of the Chuar Group is well constrained. A U-Pb zircon age of 742 +/- 6 Ma for
106 an ash bed near the top of the Walcott Member places a firm constraint on the end of Chuar
107 deposition (Karlstrom et al., 2000). Chuar strata have been placed stratigraphically below the
108 earliest (Sturtian: Hoffman and Li, 2009) glacially-influenced diamictite deposits in western
109 North America based upon correlation (e.g., Link et al., 1993; Dehler et al., 2001) and absolute
110 ages (Karlstrom et al., 2000; Fanning and Link, 2004; 2008). Further evidence for the age of
111 Chuar strata comes from the discovery of *Cerebrosphaera buickii* (Nagy et al., 2009), a proposed
112 pre-Sturtian (~777 Ma) index fossil (Hill, 2000). The Chuar Group is interpreted as being
113 internally relatively conformable (Dehler et al., 2001), and if one assumes a realistic
114 accumulation rate of 20-30 m/10⁶ years (Sadler, 1981) deposition would have commenced
115 around 800 Ma. This is consistent with the depositional duration of ~30 million years based on
116 300 m-scale cycles, each hypothesized to represent ~100 thousand years (Dehler et al., 2001).

117

118 **3.0 Methods:**

119 Fe-speciation was completed following methods outlined in Poulton and Canfield (2005).
120 This sequential extraction method allows for the quantification of ferric oxide phases such as
121 goethite, hematite (FeOx) and magnetite (FeMag), and Fe-carbonate such as siderite and ankerite
122 (FeCarb). Total Fe (FeT) was determined via a separate HF-HNO₃-HClO₄ extraction. All Fe
123 analyses were performed by atomic absorption spectroscopy. Iron sulfide minerals were
124 extracted by chromium reduction following Canfield et al. (1986). Pyrite Fe (FePy) was
125 determined gravimetrically after trapping the sulfide liberated during chromium digestion as
126 Ag₂S. We adopt a conservative estimate of uncertainty at ~4 % (relative standard deviation),

127 which reflects the external reproducibility of the extraction techniques (Canfield et al., 2008).
128 Carbonate-associated sulfate was extracted following a modified Burdett et al. (1989) method, as
129 summarized in Gill et al. (2008). Carbonate powders were rinsed twice with DI water, treated
130 with hypochlorite, rinsed two more times with DI water, and dissolved with 4N HCl. After
131 filtration, sulfate was precipitated with addition of a concentrated BaCl₂ solution. Sulfur isotope
132 analyses of Ag₂S and BaSO₄ were performed on a ThermoFinnigan Delta Plus by conversion to
133 SO₂ with a standard reproducibility of 0.2‰.

134 Minerals extracted via the sequential Fe technique are considered highly reactive towards
135 (bio)geochemical cycling during deposition and early diagenesis (Canfield et al., 1992; Poulton
136 et al., 2004b). After the inclusion of any Fe that has been converted to sulfides, this suite is
137 operationally defined as the highly reactive Fe pool (FeHR = FeOx + FeMag + FeCarb + FePy).
138 The remaining Fe (i.e. FeT – FeHR) includes Fe in clay minerals and associated with other
139 silicates; it is essentially unreactive on the timescales associated with deposition and early
140 diagenesis (here termed FeU; Raiswell and Canfield, 1996; 1998; Poulton and Raiswell, 2002).

141

142 **4.0 Results**

143 FeT in Chuar samples is unexceptional (Fig. 3, Table S1 in supplemental material). Two
144 anomalously enriched samples notwithstanding, the lower ~ 1200m of Chuar stratigraphy
145 records low mean Fe concentrations of ~ 2 wt%. The upper 400m, and especially the interval
146 1200-1400m, contains slightly less Fe, averaging ~1.5 wt%. On average, 64 % of FeT
147 throughout the Chuar Group resides in the operationally defined unreactive phase (FeU).
148 Oxidized Fe (FeOx) generally constitutes a small proportion of both the total Fe budget
149 (FeOx/FeT; average 5 %) and the FeHR pool (FeOx/FeHR ~9 %), although there are notable
150 relative enrichments of FeOx in a few intervals, particularly toward the top of the succession
151 (Figure 3). Magnetite is also a minor component, accounting for 9% of the FeHR pool
152 (FeMag/FeHR) and 3% of FeT (FeMag/FeT).

153 Iron carbonate (FeCarb) comprises the largest fraction of the highly reactive Fe budget
154 through much of the succession; however, in terms of FeT, FeCarb contents are rather variable,
155 with FeCarb/FeT varying from 74% down to 2% (average 30%). The remainder of the reduced
156 FeHR pool is pyrite (FePy). Pyrite concentrations are low through the lower km of the Chuar
157 succession, generally only contributing ~0.5 % of total Fe (FePy/FeT) and 1.5 % of the FeHR

158 pool (FePy/FeHR). The interval from 1200-1600m, however, records marked pyrite enrichment,
159 with FePy concentrations of up to 3 wt% (FePy/total rock). In these horizons, FePy dominates
160 the FeHR pool.

161 For samples from which sulfide was successfully extracted, pyrite $\delta^{34}\text{S}$ values range
162 widely, from 19.4 to -48.3 ‰ (Figure 4). Variability is much greater over the lower ~1000m of
163 the stratigraphy; values through the upper ~ 400 m cluster around a mean of 9.25‰ ($\pm 6.8\%$).
164 Sulfate sulfur, the redox complement to pyrite, was successfully extracted from 12 carbonate
165 beds within the Chuar succession (see Table S2 in supplemental material); concentrations and
166 $\delta^{34}\text{S}$ values range from 37 to 695 ppm and 2.10 to 24.57‰, respectively (Figure 4).

167

168 **5.0 Discussion**

169 *5.1 Chuar water-column chemistry:*

170 Anoxia was common in subsurface water masses of Proterozoic oceans, and in this
171 respect the Chuar basin appears typical. Total iron concentrations are slightly lower than
172 average shale composition (Turekian and Wedepohl, 1961), but not inconsistent with the ranges
173 reported in other Neoproterozoic studies (Canfield et al., 2008). Empirically, FeHR/FeT values
174 greater than 0.38 reflect deposition under anoxic conditions, whereas significantly lower values
175 generally suggest oxic bottom water (Canfield et al., 1992; Raiswell and Canfield, 1998;
176 Raiswell et al., 2001; Poulton and Raiswell, 2002). FeHR enrichment during anoxic deposition
177 reflects enhanced rates of FeHR precipitation (pyrite in sulfidic basins or ferric oxides, magnetite
178 or siderite in ferruginous basins) from anoxic water masses. As Figure 4 shows, FeHR/FeT is
179 variable throughout the Chuar Group, fluctuating repeatedly around the 0.38 threshold value.
180 Values are more regularly above the modern oxic water column average of 0.26 (Poulton and
181 Raiswell, 2002) and often fall in the equivocal range between definitive ‘anoxia’ and modern
182 oxic sediment. Anoxia is most prominent in the deepest waters, represented by the Awatubi and
183 Walcott members, but is also common in shallow shelf environments -- waters that would have
184 been below the mixed layer only under unusual shoaling of this boundary.

185 As our analyses are on outcrop samples, we must consider possible contributions from
186 secondary alteration by oxidative weathering, even though samples with visible surface staining
187 and Fe-oxidation were avoided. Post-depositional weathering reactions would cause the
188 speciation within the FeHR pool to change in a systematic fashion. To better understand the

189 implications of weathering-related secondary effects, we consider the two obvious end-members.
190 If we assume no oxidation of outcrop material, then the primary shale composition is that which
191 we report here. The other end-member would suggest that the Fe-oxides result from post-
192 depositional oxidative weathering, and that most of the Fe^{3+} now forming the FeOx pool was
193 originally Fe^{2+} . In the Chuar samples, FeOx contents are generally very low (Figure 3),
194 indicating that we can readily discount any significant influence of secondary oxidative
195 weathering for most of the succession. There are, however, some intervals, particularly towards
196 the top of the succession, where Fe oxides are relatively enriched. It is difficult to rule out
197 completely any influence of oxidative weathering in these cases. However, the close proximity
198 of these samples to other samples that contain appreciable ferrous carbonate and pyrite (Figure
199 3), coupled with the overall low FeOx contents for the remainder of the section, implies that
200 secondary oxidative weathering is unlikely to have exerted a strong influence on the conclusions
201 drawn here from mineralogical analyses..

202 Setting aside secondary oxidation, our Fe extraction data then suggest that for most of the
203 interval recorded by Chuar stratigraphy anoxia was accompanied by Fe^{2+} in the water column.
204 This conclusion is derived from the relationship between unsulfidized iron and pyrite
205 abundances, or FePy/FeHR (Fig. 4). When FePy/FeHR exceeds 0.8, euxinic conditions are
206 inferred, whereas ferruginous conditions are suggested for lower ratios (Anderson and Raiswell,
207 2004; Poulton et al., 2004b). Note that the classification as ferruginous or euxinic does not carry
208 implications for the absolute concentrations of Fe^{2+} or S^{2-} ; it simply specifies the relative
209 abundances of the two. That noted, most anoxic Chuar samples record a strongly ferruginous
210 signature ($\text{FePy}/\text{FeHR} \ll 0.8$ and often near zero); however, deep-water deposits of the upper
211 Awatubi and Walcott members contain increased pyrite contents and FePy/FeHR that, through a
212 short interval at least, exceeds 0.8. As such, the upper Awatubi and lower Walcott members are
213 interpreted to reflect enhanced diagenetic pyrite formation during a short-lived episode of
214 euxinia in the Walcott Member. As a whole, the chemostratigraphic record of the Chuar Group
215 suggests a basin in which anoxia was common, with predominantly ferruginous conditions
216 interrupted transiently by euxinia.

217

218 *5.2. Global versus local controls on redox profile*

219 The redox history of the Chuar basin probably reflects both global and basinal influences,
220 and it is important to try to distinguish between the two. The oxygen content of the surface
221 mixed layer (10s to 100s of meters) is a direct function of exchange and equilibration with the
222 atmosphere, and as such, will be controlled by atmospheric P_{O_2} and sea surface temperature. P_{O_2}
223 is a global feature whereas temperature will vary with latitude. Low paleolatitudes for Chuar
224 deposition suggest warm surface waters, possibly warmer than the $\sim 25^\circ\text{C}$ of comparable modern
225 waters, but unlikely to have been much above 40°C , given the diversity of eukaryotic organisms
226 recorded in Chuar rocks. In seawater, oxygen solubility is only about 20% lower at 40°C than at
227 25°C (Sarmiento and Gruber, 2006). Thus, by itself, high and fluctuating temperatures are
228 unlikely to explain the repeated establishment of anoxia in shallow waters and atmospheric P_{O_2}
229 much lower than today's seems mandated.

230 The dissolved oxygen content (DO) of subsurface water masses has additional controls.
231 Noting that density gradients strongly influence vertical exchange, the DO of deeper waters is
232 influenced by the P_{O_2} and temperature at the point where the water was last in contact with the
233 atmosphere (site of water parcel formation: Sarmiento and Gruber, 2006). Consistent with our
234 conclusions of low atmospheric O_2 , we would expect bottom waters in the Chuar basin to have
235 started with low O_2 concentrations (relative to today) at their time of formation. Additionally,
236 however, DO reflects the downward flux of organic carbon (OC) from surface waters. Aerobic
237 respiration of imported OC will reduce the DO pool in subsurface water masses, and if the OC
238 flux exceeds the DO supply, anoxia will develop and organic remineralization will continue
239 through anaerobic pathways. Because of its high ATP yield and thermodynamic gain, aerobic
240 respiration will be favored when oxygen is available. In the absence of oxygen, alternative
241 oxidants will be employed in a predictable order based on energy yield: NO_3^- , then Fe^{3+} , SO_4^{2-} ,
242 and finally CO_2 (methanogenesis).

243 Globally averaged, the oxygen content of the modern ocean is quite high, since today's
244 atmosphere contains $\sim 20\%$ O_2 . As a result, nitrate and sulfate levels are also high, whereas iron
245 concentrations are low. Regionally, however, the subsurface oxygen minimum zone (OMZ) can
246 experience extreme oxygen depletion, often associated with areas of upwelling. As outlined
247 above, delivery of nutrient-rich waters fuels primary production, and the ensuing export of OC to
248 the OMZ can draw down local oxygen via aerobic respiration. Whether oxygen-depleted waters
249 become sulfidic or not depends on complex interactions among primary production, OC, and the

250 nitrogen cycle (Meyer and Kump, 2008; Canfield, 2006). In today's oceans, however, anoxic
251 waters are occasionally, though not commonly sulfidic and rarely if ever ferruginous.

252 In contrast, during the Archean Eon, when atmospheric P_{O_2} was exceedingly low, water
253 masses would have been anoxic from top to bottom. In consequence, NO_3^- and SO_4^{2-} levels must
254 have been low, and in contrast to today, iron would have played a dominant role in ocean
255 chemistry and the carbon cycle (e.g., Canfield, 2005; Fischer and Knoll, 2009). Following the
256 Great Oxidation Event at ~ 2.4 Ga (Holland, 1984; Farquhar et al., 2000), oxidative weathering of
257 sulfides and greater riverine influxes of sulfate would have caused marine sulfate abundance to
258 increase, and by ~ 1800 Ma it appears that sulfate levels had risen enough for sulfide generated
259 during bacterial sulfate reduction to titrate out the dissolved iron load (Canfield, 1998; Poulton et
260 al., 2004a). Euxinia ensued, was likely common in subsurface waters (Shen et al., 2002, 2003)
261 and may have persisted until the hypothesized Neoproterozoic return of ferruginous conditions
262 (Canfield et al., 2008). How do data from the Chuar Group constrain our thinking on the latter
263 transition?

264

265 *5.3 The Chuar Basin Fe cycle:*

266 The presence of both ferruginous and euxinic conditions recorded in the Chuar Group
267 requires explanation, as the occurrence of these water chemistries is generally considered to be
268 mutually exclusive and under the control of global fluxes operating on geological timescales.
269 As evidence for ferruginous waters is persistent and sulfidic waters transient, we can ask two
270 questions. What conditions would sustain ferruginous conditions in subsurface waters? And
271 what perturbation could push these water masses toward euxinia?

272 The dominance of a particular water-column chemistry must relate to the delicate balance
273 between Fe and S in seawater (Poulton et al., 2004a; Canfield et al., 2008). The residence times
274 of these elements are, in part, controlled by hydrothermal fluxes and previous research suggests
275 that the Fe:S ratio of hydrothermal effluents relates to levels of seawater sulfate (Kump and
276 Seyfried, 2005). In the absence of sulfate, Fe:S will be high. Conversely, given sufficiently high
277 sulfate, hydrothermal systems will effectively titrate out available Fe, leaving sulfur in excess.
278 Whether because of increased reactive Fe fluxes from hydrothermal ridges (Kump and Seyfried,
279 2005), long-term erosion of the surface S reservoir (Canfield, 2004), or both, the persistent
280 signature of ferruginous conditions in Chuar bottom waters suggests that regionally, at least, the

281 chemical balance was tipped in favor of iron. If the Chuar was indeed in contact with the open
282 ocean, then the local sulfate concentration will be similar to that on a larger scale, and the effects
283 of sulfate on hydrothermal Fe output in the Chuar basin may be similar to that in other locations.
284 Further research will test this hypothesis, but Chuar data do suggest that the Neoproterozoic
285 return of ferruginous conditions in subsurface waters began some 800 million years ago, in
286 association with extensive rifting and well before the Sturtian ice age and its associated iron
287 formation. In fact, our evidence for a pre-Sturtian return of iron-rich conditions helps to explain
288 the presence of iron formation associated with Sturtian glaciogenic deposits.

289 Why then do upper Chuar rocks record a transient return of sulfidic bottom waters? We
290 cannot rule out the short-lived return of S excess regionally or globally, but given the timescales
291 for weathering (the generation of sulfate) and volumetric flux of riverine inputs (delivery of
292 sulfate), a punctuated increase in sulfate for at best a few million years seems unlikely.

293 The alternative is to explain Chuar euxinia in terms of basic biogeochemical features of
294 the carbon cycle. As noted above, oxidant use in respiration will follow a pattern prescribed by
295 energy yield. Importantly, nitrate levels were probably low in Neoproterozoic oceans (Fennel et
296 al., 2005), so iron respiration would have kicked in as oxygen disappeared from subsurface
297 waters. The quantity of Fe^{3+} available for respiration would have been the summed flux of 1.)
298 Fe^{2+} oxidized at the chemocline and shuttled to depth, 2.) physically remobilized Fe-
299 (oxy)hydroxides from shelf settings, and 3.) any background terrigenous input (Lyons and
300 Severmann, 2006). More broadly, this may relate back to the relative fluxes of reactive iron to
301 sulfate into the ocean. As Fe^{3+} respiration is favored thermodynamically over sulfate respiration,
302 dissimilatory Fe reducers would have out-competed dissimilatory sulfate reducers for the initial
303 OC load. Sulfate reduction would be left with whatever OC remained after the exhaustion of
304 reactive Fe^{3+} . In the case where ample OC remained available for sulfate reduction, bacterial
305 sulfide production would slowly titrate out Fe^{2+} , incrementally shifting the basin away from
306 ferruginous conditions and toward euxinia (increasing FePy/FeT). Consistent with this
307 hypothesis, Chuar intervals characterized by ferruginous bottom waters have low TOC, whereas
308 samples enriched in pyrite are associated with high TOC. Thus, enhanced export of OC to
309 basinal waters, perhaps driven by regional upwelling, exerted a central control on bottom water
310 chemistry in the Chuar basin.

311 In summary, then, the balance between e^- acceptors and organic carbon (the most likely e^-
312 donor) exerts a second order control on water column chemistry. As discussed above, global
313 oxygenation and anoxia is tightly linked to P_{O_2} , which our data indicate was significantly lower
314 than today. On a more local scale, however, we suggest that it is the dominant mode of OC
315 remineralization that would drive a basin or shelf environment towards ferruginous or euxinic
316 conditions. Thus, understanding basinal water chemistry can be reduced to tracking the
317 biogeochemical relationships among carbon, iron and sulfur.

318

319 *5.4. The sulfur isotope record:*

320 Sulfur isotope analyses of sedimentary sulfides in Chuar Group samples (Fig. 4) display a
321 distinctive stratigraphic pattern of variability, with the lower ~ 1000m preserving a large range of
322 isotopic compositions, while the upper 600m clusters tightly around enriched values. In fact, our
323 most depleted sample, a -48‰ pyrite from within the Tanner Member, stands as the most
324 negative $\delta^{34}S$ value yet observed in Precambrian sedimentary rocks (cf. Gorjan et al., 2000).
325 Values this depleted are common in the second half of the Phanerozoic Eon but rare in older
326 rocks (including the remainder of the Chuar sulfides). A majority of the sulfate-pyrite pairs
327 extracted from carbonate beds in the lower ~1000m of the Chuar Group suggests a $\Delta^{34}S$
328 ($\delta^{34}S_{\text{sulfate}} - \delta^{34}S_{\text{sulfide}}$) of ~ 25‰, and the complementary pyrite record (extracted from shale) is
329 consistent with this result. This magnitude of fractionation is characteristic for Neoproterozoic
330 deposits (Hurtgen et al., 2005; Fike et al., 2006). Though not immediately obvious, however,
331 this may suggest an unconventional relationship between isotopic fractionation and sulfate
332 concentrations.

333 Conventionally, ferruginous conditions are thought to require low concentrations of
334 seawater sulfate, as suggested, for instance, for Archean oceans (Habicht et al., 2002). It has also
335 been proposed that in order to produce larger isotopic fractionations from seawater sulfate, such
336 as the 25‰ measured here, seawater sulfate must be reasonably high (that is, at mM levels).
337 This latter relationship has been used to argue that the apparent increase in the range of $\delta^{34}S$
338 fractionations at the Archean-Proterozoic boundary and, again, in the terminal Neoproterozoic
339 mark increases in seawater sulfate concentrations (Canfield and Teske, 1996). If both
340 observations are correct, lower Chuar rocks may present slightly contradicting pieces of
341 conventional wisdom -- ferruginous conditions accompanied by larger (not Archean-like)

342 isotopic fractionations. Upon closer investigation, however, there is no strict *a priori* reason to
343 presume that ferruginous conditions require vanishingly low sulfate concentrations .

344 The overarching connection between ferruginous condition and seawater sulfate is more
345 literally a relationship between iron and sulfide, which has its own set of controls involving
346 organic carbon. Given at least moderate concentrations of seawater sulfate, such as the ~ 2-5
347 mM suggested for middle Proterozoic environments (c.f. Shen et al., 2002) an alternative means
348 of generating large $\delta^{34}\text{S}$ effects is through slow rates of sulfate reduction (for instance, Kaplan
349 and Rittenberg, 1964). This prediction is consistent with the postulated Chuar basin depositional
350 environment. Low rates of sulfate reduction mean low rates of sulfide generation, allowing a
351 ferruginous water column to remain as a dominant feature of ocean basins. Complementing this,
352 the limited fractionation observed for upper Chuar shale would reflect higher rates of sulfate
353 reduction, and/or quantitative reduction of pore-water (or water column) sulfate. In this way,
354 sulfate levels could have been low enough to favor Fe emission from hydrothermal ridges, but
355 high enough to account for the observed range of fractionations.

356

357 *5.5. Unifying biogeochemical principles:*

358 It may, in fact, be the relative fluxes of reactive Fe, sulfate sulfur, and organic carbon to
359 any given environment that exerts control on how the local biogeochemistry develops. Put
360 differently, the chemical evolution of an environment will be related to the fluxes of electron
361 acceptors (O_2 , NO_3^- , Fe^{3+} , SO_4^{2-}) and electron donors (organic carbon) available to heterotrophic
362 organisms. Although directly linked to fluxes to the ocean, for a microorganism it would be the
363 concentration of the species of interest at any given point; specifically within their
364 microenvironment. Given a choice of electron acceptor, there is a well-defined,
365 thermodynamically derived order in which microorganisms will use a specific oxidant (Froelich
366 et al., 1979; Berner, 1980; Stumm and Morgan, 1981; Amend and Shock, 2001). Oxygen is the
367 most favorable e^- acceptor, followed by NO_3^- , Fe^{3+} , and SO_4^{2-} (see Canfield et al., 2005;
368 Konhauser, 2007). Given our data suggesting relatively low P_{O_2} and similarly low levels of
369 nitrate (Fennel et al., 2005), ferric iron and sulfate would be the prominent oxidants.

370 We understand the stoichiometric relationships between iron, sulfur and organic carbon
371 in terms of dissimilatory microbial transformations (Canfield et al., 2005; Konhauser, 2007). In
372 what follows we present a series of inequalities in terms that relate OC, Fe^{3+} and SO_4^{2-} in anoxic,

373 nitrate poor environments. To begin, we adopt the stoichiometry of ferrihydrite reduction, where
374 4 moles of Fe^{3+} are reduced per mole of carbon (Konhauser, 2007). This means that the maximal
375 amount of OC remineralized by Fe^{3+} (in moles C) is equal to $\frac{1}{4}$ the flux of Fe^{3+} to that
376 environment (or $\frac{1}{4}[Fe^{3+}]_{influx}$). Thus,

377 if $\frac{\frac{1}{4}[Fe^{3+}]_{flux-in}}{[OC]_{flux-in}} > 1,$

378 then there should not be any additional electrons available, which given our example, would
379 have gone towards sulfate reduction (Canfield, 1998; Canfield et al., 2008). This would result in
380 a Fe^{2+} excess over sulfide; a ferruginous condition. Alternatively,

381 if $\frac{\frac{1}{4}[Fe^{3+}]_{flux-in}}{[OC]_{flux-in}} < 1,$

382 then there should be electrons available for sulfate reduction. The amount of OC available to
383 sulfate reducers after iron respiration is effectively $[OC]_{flux-in} - \frac{1}{4}[Fe^{3+}]_{flux-in}$. For an environment
384 to become euxinic and titrate out all the iron as pyrite, however, the amount of sulfide produced
385 must exceed twice the Fe^{2+} produced, or $2[Fe^{3+}]_{influx}$. Unlike iron respiration, sulfate reduction
386 remineralizes 2 moles of OC per mole sulfate. Thus, when put in terms of moles OC, for sulfide
387 production to exceed twice Fe^{2+} production (to satisfy pyrite formation) would require 16 times
388 more OC be remineralized via sulfate reduction than iron reduction. For instance, if 1 mole of
389 OC consumes all the Fe^{3+} (which here would be 4 moles Fe^{3+}), 16 additional moles (or 17 total
390 moles OC) will be necessary to produce adequate sulfide to drive euxinia. Placed back in terms
391 of measurable fluxes, euxinia then requires the influx of OC exceed $4\frac{1}{4}$ times the flux of Fe^{3+} to
392 the environment (17 moles OC per 4 moles Fe).

393 From the above relationships we conclude that for sulfide to be the dominant reduced
394 species, there must be enough available OC to consume all the Fe^{3+} and produce the quantity of
395 sulfide necessary to overwhelm the standing Fe^{2+} pool. In examining the modern marine system,
396 we find that influxes of FeHR and S to the ocean are of the same order of magnitude (10^{12}
397 mol/yr; Raiswell et al., 2006; Turchyn and Schrag, 2004, respectively), perhaps even favoring
398 iron. The sedimentary remineralization of OC has also been estimated (10^{14} mol C/yr: Canfield,
399 1993), and in comparing these fluxes in the context of the inequalities proposed above, it is
400 easier to understand why we observe euxinia accompanying oxygen deficient settings rather than
401 ferruginous waters ($[OC]_{flux-in} \gg Fe^{3+}_{flux-in}$). For ferruginous conditions to prevail in the

402 Neoproterozoic would then require primary production be much lower, FeHR inputs (perhaps
403 associated with hydrothermal activity) must have been much greater, or both. As the
404 establishment of euxinia also requires S in excess of Fe, we reassert that net Fe:S ratios of inputs
405 to the ocean will carry an important control. Overall, these predictions about the interplay
406 between C, S and Fe extend well beyond studies of Neoproterozoic ocean chemistry. For
407 instance, similar arguments could explain the transient development of sulfidic water masses in
408 the latest Archean Mount McRae Shale, given available sulfate (Reinhard et al., 2009).

409 Moving beyond assaying the balance of euxinia and ferruginous conditions, we can
410 extend this approach to develop isotopic tests of various relationships between OC and sulfate.
411 Here, these inequalities pertain to the specific behavior of sulfate reduction. We begin with the
412 condition:

413
$$\text{if } \frac{[SO_4^{2-}]_{local}}{2\left([OC]_{flux-in} - \frac{1}{4}[Fe^{3+}]_{flux-in}\right)} < 1,$$

414 where the denominator represents the stoichiometric amount of carbon required to reduce sulfate
415 and the environment is net sulfate limiting. In this case, and where OC is readily available,
416 sulfate reduction rates should be high until the sulfate reservoir is exhausted. High rates of
417 reduction generally lead to low $\delta^{34}S$ fractionations. Similarly, if sulfate is limited, environments
418 tend to record the quantitative reduction of seawater sulfate, the result of which is enriched $\delta^{34}S$
419 values. These two scenarios are likely indistinguishable in the rock record, but fortunately stem
420 from the same initial condition - sulfate limitation. Alternatively,

421
$$\text{if } \frac{[SO_4^{2-}]_{local}}{2\left([OC]_{flux-in} - \frac{1}{4}[Fe^{3+}]_{flux-in}\right)} > 1,$$

422 then the environment is net electron limited. Under conditions where organic carbon is not as
423 readily available (and possibly exhausted), sulfate reduction rates would be lower and
424 fractionation would increase.

425

426 *5.6. Implications for paleobiology*

427 Like geochemical proxies, fossils in Chuar rocks probably reflect both basinal and global
428 influences. Lower Chuar strata preserve diverse microfossils of probable eukaryotic origin
429 (Vidal and Ford, 1986; Nagy et al., 2009), but similar fossils are uncommon in upper Chuar
430 strata (Nagy et al., 2009). Evidence for persistent bottom-water anoxia throughout the Chuar

431 strata suggests that whatever the affinity of these fossilized organisms, they were likely
432 planktonic in nature. The stratigraphic distribution of Chuar fossils has been interpreted to
433 reflect a eutrophic event (Nagy et al., 2009) that correlates with observed increases in TOC, an
434 enrichment in the $\delta^{13}\text{C}$ of organic carbon (Dehler et al., 2005) and the onset of euxinia (this
435 study). The marked transition from ferruginous to euxinic conditions in the upper Chuar Group
436 also corresponds to two organic geochemical changes: a drop in the sterane to hopane ratio,
437 suggesting an increase in the proportional importance of prokaryotic primary producers and a
438 corresponding increase in C_{27} relative to C_{28} and C_{29} steranes (Ventura et al., 2005), suggesting a
439 shift in algal populations from predominantly green to red algae. Some red algae (for example
440 *Cyanidium*) can perform anaerobic fermentation under oxygen stress whereas the same capacity
441 has not been observed in green algae (Lafraie and Betz, 1985), potentially allowing reds to
442 persist opportunistically in the upper Chuar waters. However, given the requirement that they
443 produce enough overall biomass to influence sterane distributions, red algae in the upper Chuar
444 basin probably lived predominantly as primary producers. Upper Chuar dolomite nodules also
445 preserve a remarkable diversity of vase-shaped fossils interpreted as the tests of filose and lobose
446 testate amoebae, organisms that flourish today in organic-rich environments (Porter and Knoll,
447 2000; Porter et al., 2003).

448 Sulfide tolerance provides a possible means of explaining the stratigraphic concordance
449 of paleobiological and geochemical data. Sulfide is known to bind with cytochrome *c* oxidase,
450 the terminal electron acceptor in the mitochondrial e^- transport chain, thus inhibiting aerobic
451 respiration (Nicholls and Kim, 1982). Further, sulfide has been shown to interfere with ATP
452 production in animals (Bagarinao, 1992) and to obstruct other key enzymes, such as carbonic
453 anhydrase (Coleman, 1967). Many cyanobacteria are sulfide tolerant (Cohen et al., 1986;
454 Manske et al., 2005; also see Johnston et al., 2009), consistent with the observed distribution of
455 body and molecular fossils. Moreover, within this overall pattern, the increased abundances of
456 red versus green algae may speak directly to the higher Fe-requirement of greens (Quigg et al.,
457 2003). If we are correct in that organic carbon delivery (put differently, the availability of
458 electrons) stimulated the transition from ferruginous to euxinic, then it may in fact be local
459 nutrient availability that controlled the system.

460 Just as the basinal transition from ferruginous to sulfidic bottom waters favored
461 prokaryotic primary producers in the Chuar seaway, broader Neoproterozoic transition from

462 widespread subsurface euxinia to ferruginous water masses may have favored eukaryotic
463 expansion. A number of later Neoproterozoic successions record increased eukaryotic diversity
464 beginning ~800 Ma. Rocks of this age contain the earliest known protistan tests (Porter and
465 Knoll, 2000; Porter et al., 2003) and scales (Allison and Hilgert, 1986; fossiliferous strata now
466 known to be ca. 820-780 Ma, MacDonald et al., accepted), and in well-characterized fossil
467 assemblages, nearly 85% of described eukaryotes have no record in older rocks (Allison and
468 Hilgert, 1986; Butterfield et al., 1994; Porter et al., 2003; Butterfield, 2005; see Knoll et al, 2006,
469 for discussion of possible taphonomic influences). Finally, the oldest shale known to contain
470 abundant steranes is, in fact, from the Chuar Group (Ventura et al. 2005), and certain molecular
471 clocks for animal, fungal and charophyte green algal diversification suggest that these clades
472 originated in the same time frame (Peterson et al., 2008; Lucking et al., 2009).

473 Martin et al. (2003) proposed that widespread sulfide in the subsurface of mid-
474 Proterozoic oceans would have inhibited early eukaryotic diversification. Thus, if global, the
475 shift from predominantly euxinic to ferruginous subsurface waters in the Neoproterozoic might
476 have removed a barrier to eukaryotic radiation. That is, Neoproterozoic eukaryotic
477 diversification may owe as much to changing conditions in subsurface waters as it does to
478 increasing P_{O_2} in the atmosphere and surface waters. This hypothesis can be tested by detailed
479 experimentation with eukaryotic organisms and geochemical analyses of other fossiliferous
480 Neoproterozoic basins.

481

482 **6.0 Conclusion**

483 A majority of the Chuar Group strata records a geochemical setting perhaps unique until
484 this point in history: Archean-like ferruginous conditions accompanied by appreciable levels of
485 seawater sulfate. It is difficult to extrapolate with confidence from the interplay between
486 ferruginous and euxinic conditions within the Chuar basin to the character of the global ocean,
487 and continued work in contemporaneous basins will test our hypotheses. However, these data
488 suggest that the controls on regional ocean chemistry reflected both global (low atmospheric P_{O_2})
489 and basinal conditions, especially OC export from the surface ocean and the supplies of electron
490 acceptors for anaerobic remineralization. The driving force of OC export puts in place a
491 prediction: low OC environments should favor ferruginous conditions whereas higher OC export
492 will push the system towards euxinia. More specifically, and after the first-order control of P_{O_2} ,

493 we propose a quantitative relationship between the fluxes of reactive iron, sulfate, and organic
494 carbon to seafloor environments that will poise the system. With sulfate and iron available,
495 responsibility then falls to OC export to adjudicate the fate of anoxic ocean chemistry.

496 Where ferric iron pools were exhausted in the Chuar basin and sulfate reduction ensued,
497 rates of sulfide production were probably low, as was the fraction of sulfide re-oxidized (high f_{py}
498 values; see Canfield, 2004). This would effectively reduce the likelihood of accumulating, even
499 transiently, sulfur intermediate species that could be further oxidized, reduced, or
500 disproportionated. Complicated by the lack of other prominent sulfur utilizing microbial
501 processes, a $\delta^{34}\text{S}$ value of roughly -50‰ is challenging to explain, especially when CAS data
502 from the same member indicate that the $\delta^{34}\text{S}$ of seawater sulfate lay between 5 and 20‰ (or a
503 $\Delta^{34}\text{S}$ between 55-70‰). As such a $\Delta^{34}\text{S}$ exceeds conventional understanding of maximum
504 fractionation associated with sulfate reduction (Harrison and Thode, 1958), continued research
505 on the specific isotopic capability of sulfate reducing bacteria is needed (for instance, see
506 Johnston et al., 2007). We leave open the possibility that the observed fractionations are
507 primarily recording the activity of sulfate reducing bacteria.

508 In general, Chuar data contribute to an emerging picture of the Neoproterozoic Earth as a
509 world in flux. Geochemical data from the Chuar Group support the hypothesis that a return to
510 ferruginous chemistry in subsurface waters long predated the Ediacaran transition to more fully
511 oxygenated oceans (Canfield et al., 2008). In fact, evidence for pre-Sturtian iron-rich conditions
512 also helps resolve questions surrounding the resurgence of iron formation in Sturtian glacial
513 deposits. Indeed, our data suggest that this return began some 800 million years ago, more or
514 less coincident with paleogeographic (Kirschvink, 1992) and Sr-isotopic data (Veizer and
515 Compston, 1976; Asmerom et al., 1991; Halverson et al., 2007) that indicate widespread rifting
516 of the Rodinian supercontinent. Increases in rift-related sediment burial throughout the
517 Cryogenian and a potentially increased contribution from oxygenic photosynthesis to primary
518 production during this time (Johnston et al., 2009), may also help to explain the variability in
519 $\delta^{13}\text{C}$ records and why this period was so vulnerable to climatic perturbations. Thus, tectonics,
520 climatic change, redox transition and biological evolution may well be intricately interwoven
521 strands of the dynamic Neoproterozoic Earth system (e.g., Knoll, 1992). The extent to which
522 Chuar strata faithfully and fully represent the global ocean is unclear, but hypotheses inspired by
523 Chuar data are testable with geochemical reconstructions targeting contemporaneous strata.

524
525
526
527
528
529
530
531
532

Acknowledgements:

We are grateful for early conversations with G. Halverson, N. Tosca, P. Cohen, T. Lyons and R. Raiswell. Financial support was provided by NASA (NNX07AV51G: DTJ, JH, AHK), Microbial Science Institute at Harvard (DTJ), Danmark's Grundforskningsfond (DEC). The original sampling was made possible by the NSF (EAR9706541, AHK).

533

534 **Figure 1:** A geological map showing outcrop distribution of the Chuar Group, modified from
535 Porter and Knoll (2000), where G. C. SGp. notes the Grand Canyon Supergroup.

536

537 **Figure 2:** Integrated stratigraphy is modified from Dehler et al. (2005), whereas interpretations
538 of paleowater depth are adopted from Dehler et al.(2001). The Sixtymile Formation is noted as
539 "S.m. Fm.", the Nankoweap Formation is noted as "Nan. Fm.", the Duppa member is noted as
540 "Dup.", and the Carbon Butte member is noted as "C.B.". The age constraint at the top of the
541 composite section is from Karlstrom et al.(2000). Samples analyzed here are the same as
542 presented in those previous studies. Composite stratigraphy with carbon isotope compositions
543 ($\delta^{13}\text{C}$) of organic matter and carbonate, as well as total organic carbon contents (TOC) are from
544 Dehler, (2001) and Dehler et al. (2005).

545

546 **Figure 3:** Composite stratigraphy with new iron speciation data from this study. From left to
547 right, we list total Fe content (in weight %), and the relative proportion of Fe residing in
548 siliciclastic and non-siliciclastic phases (unreactive and reactive phases), reduced phases, mixed
549 valence phases, and oxidized phases. Extraction methods are described in the text. Most
550 relevant to the questions of interest are the highly reactive Fe fraction (FeHR/FeT) and the
551 reduced Fe phase, within which the reactive Fe pool resides (FeCarb or FePy).

552

553 **Figure 4:** Composite stratigraphy listing sulfur isotope data and Fe relationships that provide
554 information about paleo-redox and water column chemistry. The FeHR/FeT is a measure of
555 oxygenation, where values > 0.38 suggests anoxia (solid black line). Also listed is the modern
556 average (dashed gray line). Samples are colored to represent anoxic settings (black), oxic
557 settings (light gray), and values where a more conservative, equivocal interpretation is applied

558 (white). The center frame lists values of FePy/FeHR, which represents the fraction of Fe²⁺
559 bound as sulfide, and where values > 0.80 suggest euxinia (anoxic and sulfide containing), and
560 are represented in black. White data that fall below the 0.80 threshold suggest ferruginous
561 conditions. The right-hand frame records the δ³⁴S values of sulfides (circles) and sulfate
562 (diamonds) samples. Sedimentary sulfide extracted from shale are listed in black, whereas
563 sulfide extracted along with CAS (the sulfate presented) are listed in white. Finally, the
564 fractionation between sulfate and sulfide, Δ³⁴S, is listed to the right.

565

566

567

567

References:

568

Allison, C.W., Hilgert, J.W., 1986. Scale microfossils from the early Cambrian of northwest Canada. *J. Paleon.* 60, 973-1015.

569

570

Anbar, A.D., Knoll, A.H., 2002. Proterozoic ocean chemistry and evolution: A bioinorganic bridge? *Science* 297 1137-1142.

573

Amend, J.P., Shock, E.L., 2001. Energetics of overall metabolic reactions of thermophilic and hyperthermophilic Archaea and Bacteria. *FEMS Microbiology Reviews* 25(2) 175-243.

574

Anderson, T.F., Raiswell, R., 2004. Sources and mechanisms for the enrichment of highly reactive iron in euxinic Black Sea sediments. *Am. J. Sci.* 304 203-233.

577

Asmerom, Y., Jacobsen, S., Knoll, A.H., Butterfield, N., Swett K., 1991. Strontium isotopic variations of Neoproterozoic seawater: implications for crustal evolution. *Geochim. Cosmochim. Acta* 55 2883-2894.

581

Bagarinao, T., 1992. Sulfide as an environmental-factor and toxicant and adaptations in aquatic organisms, *Aquatic Toxicology* 24 21-62.

583

Berner, R.A., 1980. *Early Diagenesis: a theoretical approach.* Princeton University Press, Princeton, New Jersey.

586

Burdett, J.W., Arthur, M.A., Richardson, M., 1987. A Neogene seawater sulfur isotope age curve from calcareous pelagic microfossils. *Earth Planet. Sci. Lett.* 94 189-198.

588

Butterfield, N.J., 2005. Reconstructing a complex early Neoproterozoic eukaryote, Wynniatt Formation, arctic Canada. *Lethaia* 38 155-169.

591

Butterfield, N.J., Knoll, A.H., Swett, K., 1994. Paleobiology of the Upper Proterozoic Svanbergfjellet Formation, Spitsbergen. *Fossils and Strata* 34 1-84.

594

Canfield, D.E., 1993. Organic matter oxidation in marine sediments. In: *NATO-ARW interactions of C, N, P, and S biogeochemical cycles and global change* 333-365.

597

Canfield, D.E., 1998. A new model for Proterozoic ocean chemistry, *Nature* 396 450-453.

600

Canfield, D.E., 2004. The evolution of the Earth surface sulfur reservoir. *Am. J. Sci.* 304 839-861.

602

Canfield, D.E., 2005. The early history of atmospheric oxygen: Homage to Robert A. Garrels. *Annual Review of Earth and Planetary Sciences* 33 1-36.

604

Canfield, D.E., 2006. Models of oxic respiration, denitrification and sulfate reduction in zones of coastal upwelling. *Geochim. Cosmochim. Acta* 70 5753-5765.

607

Canfield, D.E., Poulton, S.W., Knoll, A.H., Narbonne, G.M., Ross, G., Goldberg, T., Strauss, H., 2008. Ferruginous conditions dominated later Neoproterozoic deep-water chemistry. *Science* 321 949-952.

610

Canfield, D.E., Poulton, S.W., Narbonne, G.M., 2007. Late-Neoproterozoic deep-ocean oxygenation and the rise of animal life. *Science* 315 92-95.

613

Canfield, D.E., Raiswell, R., Bottrell, S., 1992. The reactivity of sedimentary iron minerals towards sulfide. *Am. J. Sci.* 292 659-683.

616

Canfield, D.E., Raiswell, R., Westrich, J.T., Reaves, C.M., Berner, R.A., 1986. The use of chromium reduction in the analysis of reduced inorganic sulfur in sediments and shales. *Chem. Geol.* 54 149-155.

619

620

621

- 622 Canfield, D.E., Teske, A., 1996. Late Proterozoic rise in atmospheric oxygen concentration inferred from
623 phylogenetic and sulphur-isotope studies. *Nature* 382 127-132.
624
- 625 Canfield, D.E. Kristensen, E., Thamdrup, B. 2005. Aquatic Geomicrobiology. *Advances in Marine Biology* 48.
626
- 627 Cloud P., 1976. Beginnings of biospheric evolution and their biogeochemical consequences. *Paleobiology* 2 351-
628 387.
629
- 630 Coleman, J.E., 1967. Mechanism of action of carbonic anhydrase - substrate sulfonamide and anion binding. *J. Biol.*
631 *Chem.* 242 5212-5235.
632
- 633 Cohen, Y., Jorgensen, B.B., Revsbech, N.P., Poplawski, R., 1986. Adaption to hydrogen sulfide of oxygenic and
634 anoxygenic photosynthesis among cyanobacteria. *App. Envi. Micro.* 51 398-407.
635
- 636 Dalziel, I.W.D., 1997. Neoproterozoic-Paleozoic geography and tectonics: Review, hypothesis, environmental
637 speculation. *Geol. Soc. Am. Bull.* 109 16-42.
638
- 639 Dehler, C.M., 2001. Facies analysis, cyclostratigraphy, and carbon-isotope stratigraphy of the Neoproterozoic
640 Chuar Group, Grand Canyon, Arizona. PhD thesis. 371 p.
641
- 642 Dehler, C.M., Elrick, M., Bloch, J.D., Crossey, L.J., Karlstrom, K.E., Des Marais, D.J., 2005. High-resolution delta
643 C-13 stratigraphy of the Chuar Group (ca. 770-742 Ma), Grand Canyon: Implications for mid-
644 Neoproterozoic climate change. *Geol. Soc. Am. Bull.* 117 32-45.
645
- 646 Dehler, C.M., Elrick, M., Karlstrom, K.E., Smith, G.A., Crossey, L.J., Timmons, J.M., 2001. Neoproterozoic Chuar
647 Group (similar to 800-742 Ma), Grand Canyon: a record of cyclic marine deposition during global cooling
648 and supercontinent rifting. *Sed. Geol.* 141 465-499.
649
- 650 Fanning, C.M., Link, P.K., 2004. U-Pb SHRIMP ages of Neoproterozoic (Sturtian) glaciogenic Pocatello Formation,
651 southeastern Idaho. *Geology* 32 881-884.
652
- 653 Fanning, C.M., and Link, P.K., 2008, Age constraints for the Sturtian Glaciation; data from the Adelaide
654 Geosyncline, South Australia and Pocatello Formation, Idaho, USA: / in/ Gallagher, S.J., and Wallace,
655 M.W., eds., Neoproterozoic extreme climates and the origin of early metazoan life: Geological Society of
656 Australia Extended Abstracts No. 91, p. 57-62.
657
- 658 Farquhar, J., Bao, H.M., Thiemens, M., 2000. Atmospheric influence of Earth's earliest sulfur cycle. *Science* 289
659 756-758.
660
- 661 Fennel, K., Follows, M., Falkowski, P.G., 2005. The co-evolution of the nitrogen, carbon and oxygen cycles in the
662 Proterozoic ocean. *Am. J. Sci.* 305 526-545.
663
- 664 Fike, D.A., Grotzinger, J.P., Pratt, L.M., Summons, R.E., 2006. Oxidation of the Ediacaran Ocean. *Nature* 444 744-
665 747.
666
- 667 Fischer, W.W., Knoll, A.H., 2009. An iron shuttle for deepwater silica in Late Archean and early Paleoproterozoic
668 iron formation. *Geol. Soc. Am. Bull.* 121 222-235.
669
- 670 Ford, T.D., Breed, W.J., 1973. Late Precambrian Chuar Group, Grand Canyon, Arizona. *Geological Society of*
671 *America Bulletin*, 84: 1243-1260.
672
- 673 Froelich, P.N., Klinkhammer, G.P., Bender, M.L., Luedtke, G.R., Heath, G.R., Cullen, D., Dauphin, P., Hammond,
674 D., Hartman, B., Maynard, V. 1979. Early oxidation of organic matter in pelagic sediments of the eastern
675 equatorial atlantic: suboxic diagenesis. *Geochim. Cosmochim. Acta* 43 1075-1090.
676

677 Gill, B.C., Lyons, T.W., Frank, T.D., 2008. Behavior of carbonate-associated sulfate during meteoric diagenesis and
678 implications for the sulfur isotope paleoproxy. *Geochim. Cosmochim. Acta* 72 4699-4711.
679

680 Habicht, K.S., Gade, M., Thamdrup, B., Berg, P., Canfield, D.E., 2002. Calibration of sulfate levels in the Archean
681 ocean. *Science*. 298 2372-2374.
682

683 Halverson, G.P., Dudas, F.O., Maloof, A.C., Bowring, S.A., 2007. Evolution of the Sr-87/Sr-86 composition of
684 Neoproterozoic seawater. *Palaeogeography Palaeoclimatology Palaeoecology* 256 103-129.
685

686 Harrison, A.G., Thode, H.G., 1958. Mechanism of the bacterial reduction of sulphate from isotope fractionation
687 studies. *Transactions of the Faraday Society* 54 84-92.
688

689 Hill, A.C., Cotter, K.L. & Grey, K. Mid-Neoproterozoic biostratigraphy and isotope stratigraphy in Australia.
690 *Precambrian Res.* **100**, 281-298 (2000).
691

692 Hoffman, P.F., and Li, Z.X., 2009. A paleogeographic context for Neoproterozoic glaciations, *Paleogeography,*
693 *Paleoclimatology, Paleocology*, doi: 10.1016/j.palaeo.2009.03.013.
694

695 Holland, H.D., 1984. *Chemical evolution of the atmosphere and oceans.* Princeton Press.
696

697 Hurtgen, M. T., Arthur, M. A., Halverson, G.P., 2005. Neoproterozoic sulfur isotopes, the evolution of microbial
698 sulfur species, and the burial efficiency of sulfide as sedimentary pyrite. *Geology* 33 41-44.
699

700 Isley, A.E., Abbott, D.H., 1999. Plume-related mafic volcanism and the deposition of banded iron formation. *J.*
701 *Geophys. Res.-Solid Earth* 104 15461-15477.
702

703 Johnston, D.T., Farquhar, J., Canfield, D.E., 2007. Sulfur isotope insights into microbial sulfate reduction: When
704 microbes meet models. *Geochim. Cosmochim. Acta* 71 3929-3947.
705

706 Johnston, D.T., Wolfe-Simon, F., Pearson, A., Knoll, A.H., 2009. Anoxygenic photosynthesis modulated
707 Proterozoic oxygen and sustained Earth's middle age. *Proc. Nat. Acad. Sci. U.S.A.* 106(40), 16925-16929.
708

709 Kaplan, I.R., Rittenberg, S.C., 1964. Microbiological fractionation of sulphur isotopes. *J. Gen. Microbio.* 34 195-
710 202.
711

712 Karlstrom, K.E., Bowring, S.A., Dehler, C.M., Knoll, A.H., Porter, S.M., Des Marais, D.J., Weil, A.B., Sharp, Z.D.,
713 Geissman, J.W., Elrick, M.B., Timmons, J.M., Crossey, L.J., Davidek, K.L., 2000. Chuar Group of the
714 Grand Canyon: Record of breakup of Rodinia, associated change in the global carbon cycle, and ecosystem
715 expansion by 740 Ma. *Geology* 28 619-622.
716

717 Kirschvink, J.L., 1992. A paleogeographic model for Vendian and Cambrian time. In: *The Proterozoic Biosphere.*
718

719 Knoll, A.H., 1992. Biological and biogeochemical preludes to the Ediacaran radiation. In: J., Lipps and P. Signor,
720 eds., *The Origin and Early Evolution of Metazoans.* Plenum, New York 53-84.
721

722 Knoll, A.H., Hates, J.M., Kaufman, A.J., Swett, K., Lambert, I.B., 1986. Secular variation in carbon isotope ratios
723 from upper Proterozoic successions of Svalbard and east Greenland. *Nature*, 321(6073) 832-838.
724

725 Knoll, A.H., Javaux, E.J., Hewitt, D., Cohen, P., 2006. Eukaryotic organisms in Proterozoic oceans. *Phil. Trans Roy.*
726 *Soc. B-Biological Sciences* 361 1023-1038.
727

728 Konhauser, K. 2007. *Introduction to Geomicrobiology.* Blackwell Publishing.
729

730 Kump, L.R., Seyfried, W.E., 2005. Hydrothermal Fe fluxes during the Precambrian: Effect of low oceanic sulfate
731 concentrations and low hydrostatic pressure on the composition of black smokers. *Earth Planet. Sci. Lett.*
732 235 654-662.

733
734 Lyons, T.W., Severmann, S. 2006. A critical look at iron paleoredox proxies: New insights from modern euxinic
735 marine basins. *Geochim. Cosmochim. Acta* 70 5698-5722.
736
737 Lafraie, M.A., Betz, A., 1985. Anaerobic fermentation in cyanidium-caldarium. *Planta* 163 38-42.
738
739 Li, Z.X., Li, X.H., Kinny, P.D., Wang, J., Zhang, S., Zhou, H. 2003. Geochronology of Neoproterozoic syn-rift
740 magmatism in the Yangtze Craton, South China and correlations with other continents: evidence for a
741 mantle superplume that broke up Rodinia. *Precambrian Research*, 122(1-4) 85-109.
742
743 Link, P. K., Christie-Blick, N., Devlin, W.J., Elston, D.P., Horodyski, R.J., Levy, M., Miller, J.M.G., Pearson, R.C.,
744 Prave, A., Stewart, J.H., Winston, D., Wright, L.A., Wrucke, C.T., 1993, Middle and Late Proterozoic
745 stratified rocks of the western U.S. Cordillera, Colorado Plateau, and Basin and Range province, *in* Reed,
746 J.C., Bickford, M.E., Houston, R.S., Link, P.K., Rankin, D.W., Sims, P.K., and Van Schmus, W.R., eds.,
747 *The Geology of North America, Volume C-2, Precambrian: Conterminous U.S.*: Boulder, Geological
748 Society of America, p. 463-595.
749
750 Lucking, R., Huhndorf, S., Pfister, D.H., Plata, E.R., Lumbsch, H.T. 2009. Fungi evolved right on track. *Mycologia*
751 101 810-822.
752
753 Macdonald, F.A., Cohen, P., Dudas, F., Schrag, D. 2009. Early Neoproterozoic siliceous scale microfossils in the
754 Tindir Group of Alaska and the Yukon Territory. *Geology*.
755
756 Manske, A.K., Glaeser, J., Kuypers, M.M.M., Overmann, J., Physiology and phylogeny of green sulfur bacteria
757 forming a monospecific phototrophic assemblage at a depth of 100 meters in the Black Sea. *Ap. Envi.*
758 *Micro.* 71 8049-8060.
759
760 Martin, W., Rotte, C., Hoffmeister, M., Theissen, U., Gelius-Dietrich, G., Ahr, S., Henze, K., 2003. Early cell
761 evolution, eukaryotes, anoxia, sulfide, oxygen, fungi first (?), and a tree of genomes revisited. *Iubmb Life*
762 55 193-204.
763
764 Meyer, K.M., Kump, L.R., 2008. Oceanic euxinia in Earth history: Causes and consequences. *Ann. Rev. Earth and*
765 *Planet. Sci.* 36 251-288.
766
767 Nagy, R.M., Porter, S.M., Dehler, C.M., Shen, Y. 2009. Pre-glacial biotic turnover in the mid-Neoproterozoic Chuar
768 Group, Grand Canyon, *Nature Geoscience* 2, 415-418.
769
770 Nicholls, P., Kim, J.K., 1982. Sulfide as an inhibitor and electron donor for the cytochrome c oxidase system. *Can.*
771 *J. Biochem.* 60 613-623.
772
773 Peterson, K.J., Cotton, J.A., Gehling, J.G., Pisani, D., 2008. The Ediacaran emergence of bilaterians: congruence
774 between the genetic and the geological fossil records. *Phil. Trans. Roy. Soc. B-Biol. Sci.* 363 1435-1443.
775
776 Porter, S.M., Knoll, A.H., 2000. Testate amoebae in the Neoproterozoic Era: evidence from vase-shaped
777 microfossils in the Chuar Group, Grand Canyon. *Paleobiology* 26 360-385.
778
779 Porter, S.M., Meisterfeld, R., Knoll, A.H., 2003. Vase-shaped microfossils from the Neoproterozoic Chuar Group,
780 Grand Canyon: A classification guided by modern testate amoebae. *J. Paleon.* 77 409-429.
781
782 Poulton, S.W., Canfield, D.E., 2005. Development of a sequential extraction procedure for iron: implications for
783 iron partitioning in continentally derived particulates. *Chem. Geol.* 214 209-221.
784
785 Poulton, S.W., Fralick, P.W., Canfield, D.E., 2004a. The transition to a sulphidic ocean similar to 1.84 billion years
786 ago. *Nature* 431 173-177.
787

788 Poulton, S.W., Krom, M.D., Raiswell, R., 2004b. A revised scheme for the reactivity of iron (oxyhydr)oxide
789 minerals towards dissolved sulfide. *Geochim. Cosmochim. Acta* 68 3703-3715.
790

791 Poulton, S.W., Raiswell, R., 2002. The low-temperature geochemical cycle of iron: From continental fluxes to
792 marine sediment deposition. *Am. J. Sci.* 302 774-805.
793

794 Poulton, S.W., Fralick, P.W., Canfield, D.E., in review. A new look at the history of late Paleoproterozoic ocean
795 chemistry. *Geology*.
796

797 Preiss, W.V., 2000, The Adelaide Geosyncline of South Australia and its significance in Neoproterozoic continental
798 reconstruction: *Precambrian Research*, v. 100, p. 21-63.
799

800 Quigg, A., Finkel, Z.V., Irwin, A.J., Rosenthal, Y., Ho, T.Y., Reinfelder, J.R., Schofield, O., Morel, F.M.M.,
801 Falkowski, P.G., 2003. The evolutionary inheritance of elemental stoichiometry in marine phytoplankton.
802 *Nature* 425 291-294.
803

804 Rainbird, R.H., Jefferson, C.W., and Young, G.M., 1996, The early Neoproterozoic sedimentary Succession B of
805 northwestern Laurentia: Correlations and paleogeographic significance. *Geological Society of America*
806 *Bulletin*, v. 108, no. 4, p. 454-470.
807

808 Raiswell, R., Canfield, D.E., 1996. Rates of reaction between silicate iron and dissolved sulfide in Peru Margin
809 sediments. *Geochim. Cosmochim. Acta* 60 2777-2787.
810

811 Raiswell, R., Canfield, D.E., 1998. Sources of iron for pyrite formation in marine sediments. *Am. J. Sci.* 298 219-
812 245.
813

814 Raiswell, R., Newton, R. N, Wignall, P.B., 2001. An indicator of water-column anoxia: Resolution of biofacies
815 variations in the Kimmeridge Clay (Upper Jurassic, UK). *J. Sed. Res.* 71 286-294.
816

817 Raiswell, R., Tranter, M., Benning, L.G. Siegert, M. De'ath, R., Huybrechts, P., Payne, T., 2006. Contributions from
818 glacially derived sediment to the global iron (oxyhydr)oxide cycle: Implications for iron delivery to the
819 oceans. *Geochim. Cosmochim. Acta* 70 2765-2780.
820

821 Reinhard, C.T., Raiswell, R. Scott, C., Anbar A.D., Lyons T.W., 2009. A Late Archean sulfidic sea stimulated by
822 early oxidative weathering of the continents. *Science* 326 713-716.
823

824 Sadler, P.M., 1981. Sediment accumulation rates and the completeness of stratigraphic sections. *Journal of*
825 *Geology* 89 569-584.
826

827 Sarmiento, J.L., Gruber, N., 2006. *Ocean biogeochemical dynamics*, Princeton University Press.
828

829 Schopf, J.W., Ford, T.D., Breed, W.J., 1973. Microorganisms from late Precambrian of Grand Canyon, Arizona.
830 *Science* 179 1319-1321.
831

832 Shen, Y.N., Canfield, D.E., Knoll, A.H., 2002. Middle Proterozoic ocean chemistry: Evidence from the McArthur
833 Basin, northern Australia. *Am. J. Sci.* 302 81-109.
834

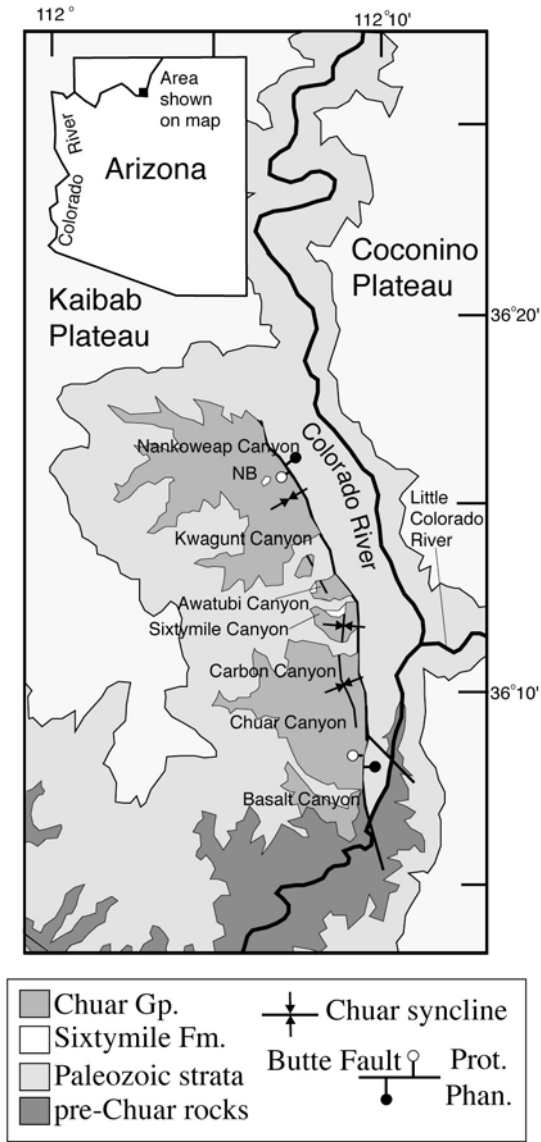
835 Shen, Y.N., Zhang, T.G., Hoffman, P.F., 2008. On the coevolution of Ediacaran oceans and animals. *Proc. Nat.*
836 *Acad. Sci. U.S.A.* 105 7376-7381.
837

838 Shen, Y., Knoll, A.H., Walter, M.R., 2003. Evidence for low sulphate and anoxia in a mid-Proterozoic marine basin.
839 *Nature* 423 632-635.
840

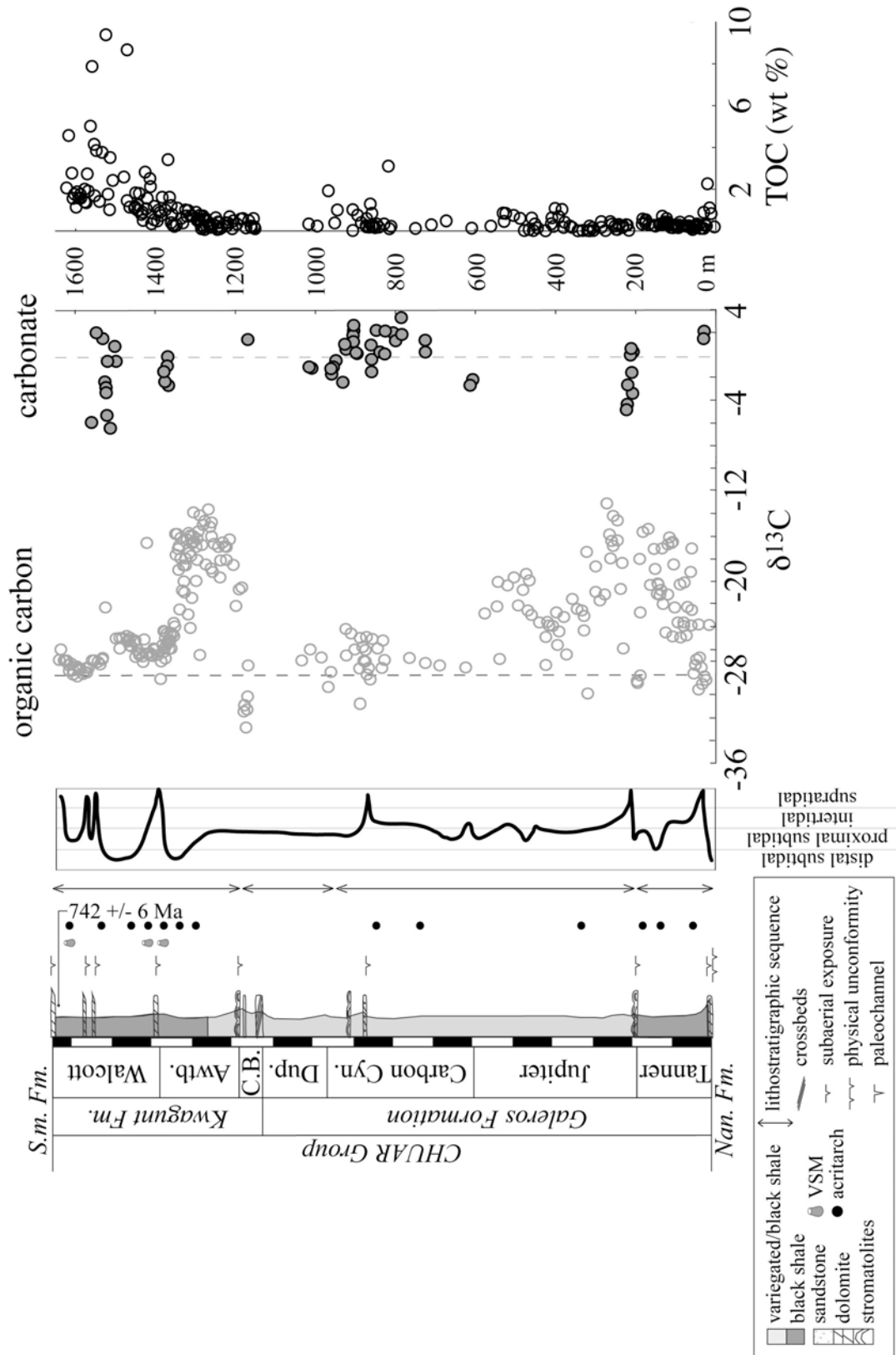
841 Stumm, W., Morgan, J.J., 1981. *Aquatic Chemistry*. John Wiley and Sons, New York.
842

- 843 Summons, R.E., Brassell, S.C., Eglinton, G., Evans, E., Horodyski, R.J., Robinson, N., Ward, D.M., 1988.
844 Distinctive hydrocarbon biomarkers from fossiliferous sediment of the late Proterozoic Walcott Member,
845 Chuar Group, Grand Canyon, Arizona. *Geochim. Cosmochim. Acta* 52 2625-2637.
846
- 847 Timmons, J.M., Karlstrom, K.E., Dehler, C.M., Geissman, J.W., Heizler, M.T., 2001. Proterozoic multistage (ca. 1.1
848 and 0.8 Ga) extension recorded in the Grand Canyon Supergroup and establishment of northwest- and
849 north-trending tectonic grains in the southwestern United States. *Geol. Soc. Am. Bull.* 113 163-180.
850
- 851 Turchyn, A.V., Schrag, D.P., 2004. Oxygen isotope constraints on the sulfur cycle over the past 10 million years.
852 *Science* 303 2004-2007.
853
- 854 Turekian, K.K., Wedepohl, K.H. 1961. Distribution of the elements in some major units of the Earth's crust. *Geol.*
855 *Soc. Am. Bull.* 72, 175-191.
856
- 857 Veizer, J., Compston, W., 1976. Sr87/Sr86 in Precambrian carbonates as an index of crustal evolution. *Geochim.*
858 *Cosmochim. Acta* 40 905-914.
859
- 860 Ventura, G.T., Kenig, F., Grosjean, E., Summons, R.E., 2005. Biomarker analysis of extractable organic matter from
861 the Neoproterozoic Kwagunt Formation, Chuar Group (~800-742 Ma). Fall AGU meeting abstracts.
862
- 863 Vidal, G., Ford, T.D., 1985. Microbiotas from the late Proterozoic Chuar Group (northern Arizona) and Uinta
864 Mountain Group (Utah) and their chemostratigraphic implications. *Precambrian Res.* 28 349-389.
865
- 866 Walker, J.C.G., Brimblecombe, P., 1985. Iron and sulfur in the pre-biogenic ocean. *Precambrian Res.* 28 205-222.
867
- 868 Weil, A.B., Geissman, J.W., Van der Voo, R., 2004. Paleomagnetism of the Neoproterozoic Chuar Group, Grand
869 Canyon Supergroup, Arizona: implications for Laurentia's Neoproterozoic APWP and Rodinia break-up.
870 *Precambrian Res.* 129 71-92.

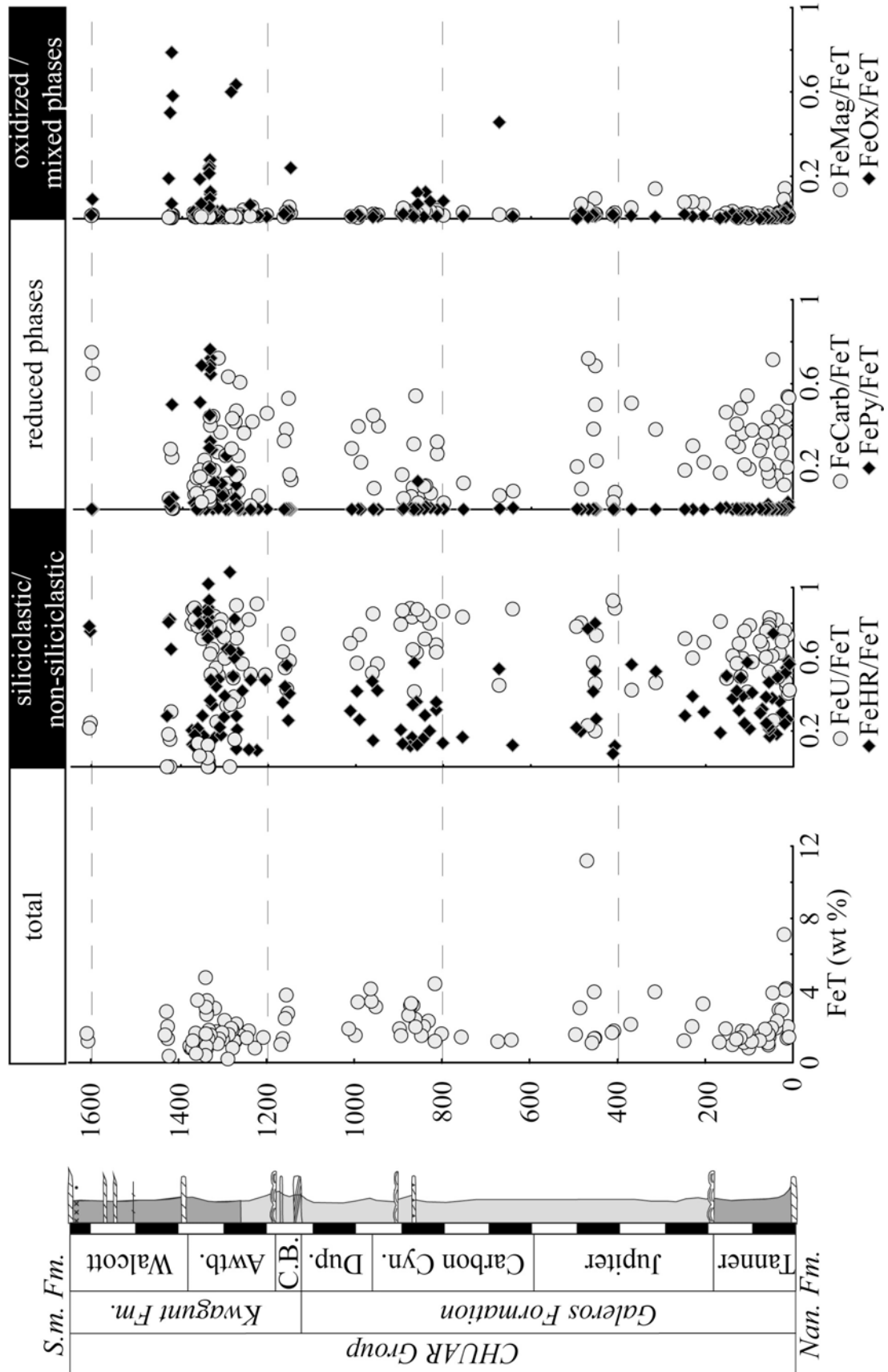
Johnston et al., (CHUAR): Figure 1



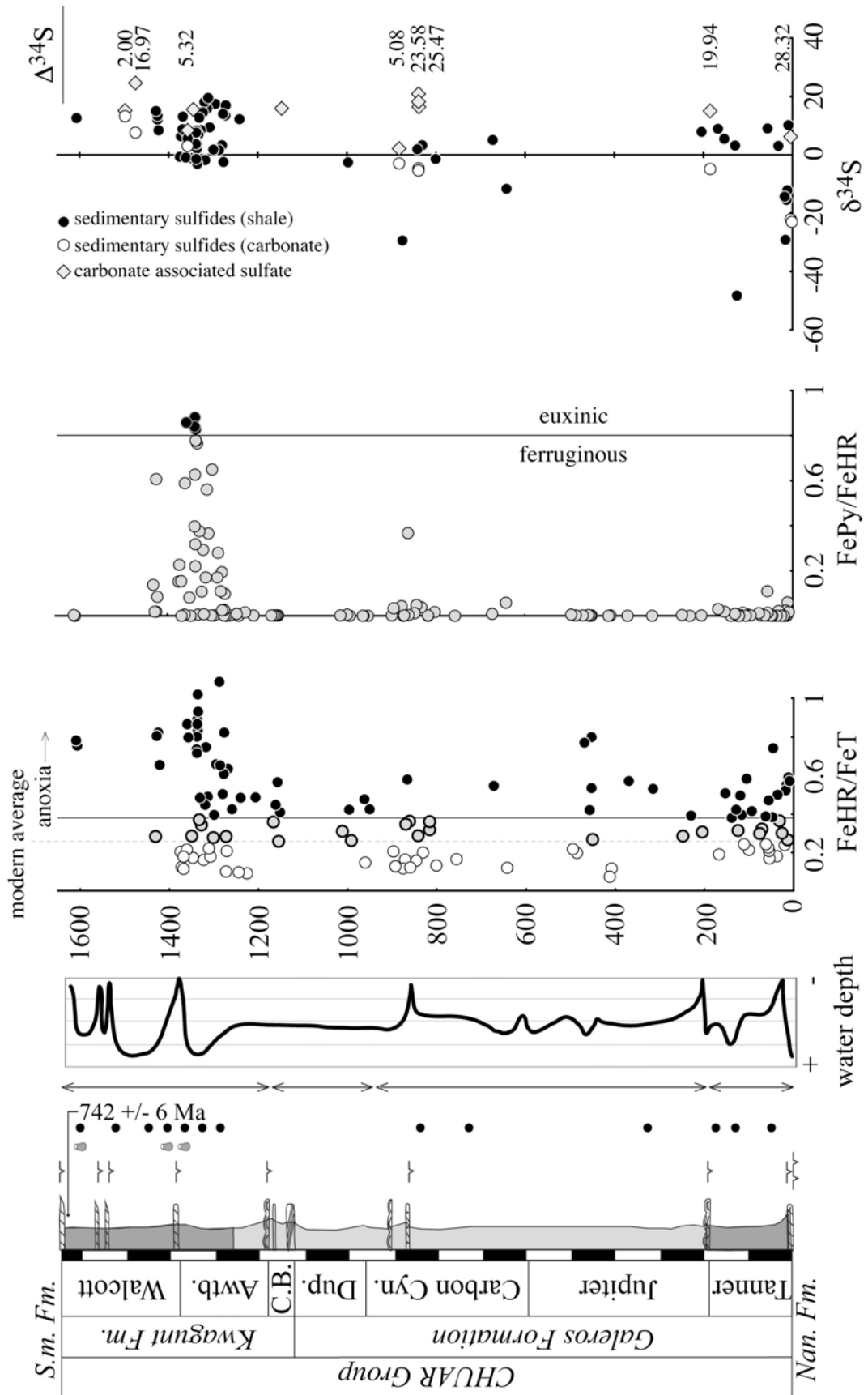
Johnston et al (CHUAR) Figure 2



Johnston et al., (CHUAR): Figure 3



Johnston et al., (CHUAR): Figure 4



Member	section	depth	$\delta^{34}\text{S}$	FeT	FeHR	FeU	FeHR/FeT	FeP/FeHR
Tanner	10	12	-12.21	2.01	1.19	0.41	0.59	5.96E-02
Tanner	10	13.5	-15.49	1.36	0.36	0.73	0.27	2.78E-07
Tanner	10	16	-29.10	4.12	2.27	0.45	0.55	2.24E-02
Tanner	10	17.5	-14.33	4.03	2.11	0.48	0.52	4.74E-08
Tanner	10	31.5	2.97	2.94	1.07	0.64	0.36	2.10E-02
Tanner	10	38	-	1.93	0.35	0.82	0.18	2.87E-07
Tanner	10	54	-	1.43	0.24	0.83	0.17	1.75E-03
Tanner	10	55.5	-	0.97	0.20	0.79	0.21	4.32E-03
Tanner	10	57	-	1.09	0.24	0.78	0.22	1.08E-01
Tanner	10	61.5	-	1.81	0.44	0.76	0.24	2.77E-03
Tanner	10	71	-	1.55	0.50	0.68	0.32	8.81E-04
Tanner	10	100.5	-	0.81	0.17	0.79	0.21	5.17E-03
Tanner	10	111.5	-	1.11	0.27	0.76	0.24	1.31E-02
Tanner	10	116	-	1.76	0.70	0.60	0.40	1.24E-03
Tanner	10	124.5	-48.30	1.32	0.41	0.69	0.31	2.42E-07
Tanner	10	138.5	-	0.99	0.38	0.62	0.38	2.66E-07
Tanner	11	9	10.17	1.41	0.81	0.43	0.57	1.60E-02
Tanner	11	20	-	7.11	1.70	0.76	0.24	2.51E-04
Tanner	11	26	-	2.90	0.87	0.70	0.30	4.94E-04
Tanner	11	36	-	2.30	1.15	0.50	0.50	7.40E-04
Tanner	11	46	-	3.86	2.86	0.26	0.74	3.02E-04
Tanner	11	48	-	1.92	0.74	0.62	0.38	1.14E-03
Tanner	11	56	9.04	1.58	0.74	0.53	0.47	1.28E-02
Tanner	11	63	-	1.85	0.72	0.61	0.39	1.21E-03
Tanner	11	76	-	1.23	0.37	0.70	0.30	1.14E-02
Tanner	11	94	-	1.17	0.49	0.59	0.41	1.78E-03
Tanner	11	105	-	1.73	1.01	0.42	0.58	4.24E-04
Tanner	11	120	-	1.37	0.68	0.50	0.50	6.36E-04
Tanner	11	129	3.09	1.30	0.55	0.58	0.42	7.75E-03
Tanner	11	153	5.41	1.89	0.96	0.49	0.51	1.80E-02
Tanner	11	167	8.86	1.13	0.21	0.81	0.19	2.98E-02
Jupiter	9a	204.5	7.87	3.26	1.00	0.69	0.31	1.30E-03
Jupiter	9a	230	-	2.00	0.78	0.61	0.39	5.56E-04
Jupiter	9a	248	-	1.22	0.35	0.71	0.29	2.51E-03
Jupiter	9a	315	-	3.93	2.09	0.47	0.53	4.79E-08
Jupiter	9a	370	-	2.12	1.21	0.43	0.57	8.28E-08
Jupiter	9a	408	-	1.76	0.20	0.88	0.12	2.12E-03
Jupiter	9a	412	-	1.67	0.12	0.93	0.07	8.13E-07
Carbon Canyon	3	801	-1.47	1.60	0.21	0.87	0.13	1.68E-02
Carbon Canyon	3	816	-	4.38	1.40	0.68	0.32	7.66E-04
Carbon Canyon	3	816	-	1.19	0.43	0.64	0.36	1.01E-03
Carbon Canyon	3	831	3.31	2.32	0.46	0.80	0.20	3.73E-02
Carbon Canyon	3	842	1.92	2.00	0.57	0.71	0.29	4.76E-02
Carbon Canyon	3	861	-	2.41	0.87	0.64	0.36	3.68E-01
Carbon Canyon	3	866	-	3.18	1.84	0.42	0.58	3.49E-03
Carbon Canyon	3	871.5	-	3.17	0.52	0.84	0.16	8.17E-04
Carbon Canyon	3	875.5	-29.33	2.63	0.30	0.88	0.12	4.30E-02
Carbon Canyon	3	897	-	1.88	0.39	0.79	0.21	1.12E-03
Carbon Canyon	9a	451	-	1.35	0.36	0.73	0.27	1.20E-03
Carbon Canyon	9a	453	-	3.93	3.15	0.20	0.80	2.70E-04
Carbon Canyon	9a	453	-	1.33	0.71	0.47	0.53	1.23E-03
Carbon Canyon	9a	457.5	-	1.09	0.46	0.58	0.42	3.72E-03
Carbon Canyon	9a	469.5	-	11.20	8.63	0.23	0.77	9.95E-04
Carbon Canyon	9a	485.5	-	3.04	0.60	0.80	0.20	1.77E-03
Carbon Canyon	9a	495.5	-	1.55	0.34	0.78	0.22	5.05E-03

Member	section	depth	$\delta^{34}\text{S}$	FeT	FeHR	FeU	FeHR/FeT	FeP/FeHR
Carbon Canyon	9a	642	-11.62	1.26	0.15	0.88	0.12	5.73E-02
Carbon Canyon	9a	672.5	5.08	1.17	0.64	0.45	0.55	7.89E-03
Carbon Canyon	9a	756	-	1.41	0.23	0.83	0.17	4.27E-07
Carbon Canyon	9a	846.5	-	1.49	0.23	0.84	0.16	1.10E-02
Carbon Canyon	9a	860	-	1.99	0.24	0.88	0.12	3.53E-03
Carbon Canyon	9a	870	-	3.28	1.13	0.65	0.35	1.41E-03
Carbon Canyon	9a	893	-	1.51	0.19	0.87	0.13	3.36E-02
Duppa	SP	951	-	3.10	1.32	0.58	0.42	6.53E-04
Duppa	SP	961	-	3.40	0.50	0.85	0.15	2.00E-07
Duppa	SP	962.5	-	4.08	1.94	0.52	0.48	5.14E-08
Duppa	SP	991.5	-	3.35	0.88	0.74	0.26	1.14E-07
Duppa	SP	997	-2.61	1.51	0.64	0.58	0.42	5.67E-03
Duppa	SP	1012	-	1.88	0.59	0.69	0.31	1.75E-03
Awatubi	4	1151.5	-	2.74	1.12	0.59	0.41	1.17E-03
Awatubi	4	1154.5	-	3.75	0.97	0.74	0.26	1.44E-03
Awatubi	4	1157.5	-	2.46	1.39	0.43	0.57	2.26E-03
Awatubi	4	1162	-	1.34	0.60	0.55	0.45	2.39E-03
Awatubi	4	1167	-	1.01	0.36	0.64	0.36	2.37E-03
Awatubi	4	1207	-	1.39	0.68	0.51	0.49	1.91E-03
Awatubi	4	1226	-	0.82	0.08	0.91	0.09	1.53E-02
Awatubi	4	1240.5	12.24	1.76	0.85	0.51	0.49	1.17E-07
Awatubi	4	1259.5	-	1.49	0.63	0.58	0.42	1.55E-03
Awatubi	4	1268.5	-	2.14	1.36	0.36	0.64	6.80E-04
Awatubi	4	1273	-	1.23	0.35	0.72	0.28	2.48E-03
Awatubi	4	1295.5	17.41	2.36	1.55	0.34	0.66	1.25E-03
Awatubi	4	1313.5	15.86	1.72	0.84	0.51	0.49	1.70E-01
Awatubi	4	1319.5	18.06	1.18	0.53	0.55	0.45	2.93E-01
Awatubi	4	1323	14.49	1.27	0.20	0.84	0.16	1.08E-01
Awatubi	4	1331	12.74	1.80	0.87	0.52	0.48	5.06E-03
Awatubi	4	1271.5	16.96	1.20	0.25	0.79	0.21	9.79E-02
Awatubi	4	1273	13.46	1.20	0.12	0.90	0.10	2.66E-02
Awatubi	4	1277.5	13.92	1.82	1.11	0.39	0.61	1.93E-01
Awatubi	4	1280	3.20	1.91	0.96	0.50	0.50	1.09E-01
Awatubi	4	1286.5	1.64	1.57	1.02	0.35	0.65	2.79E-01
Awatubi	4	1299.5	1.74	1.30	0.51	0.61	0.39	6.49E-01
Awatubi	4	1301.5	-	1.66	0.46	0.72	0.28	2.13E-03
Awatubi	4	1308	9.37	1.32	0.23	0.82	0.18	3.65E-01
Awatubi	4	1311	19.40	1.05	0.23	0.78	0.22	5.60E-01
Awatubi	4	1318	-1.89	3.01	2.25	0.25	0.75	6.23E-03
Awatubi	4	1328	8.49	1.54	0.53	0.66	0.34	3.76E-01
Awatubi	4	1333	6.92	1.34	0.50	0.63	0.37	7.66E-01
Walcott	4	1347.5	-	1.42	0.25	0.83	0.17	4.07E-07
Walcott	4	1372.5	6.39	0.81	0.10	0.88	0.12	2.26E-01
Walcott	4	1374.5	-0.74	0.94	0.19	0.80	0.20	1.52E-01
Walcott	4	1606.5	12.63	1.19	0.90	0.24	0.76	1.11E-07
Walcott	8	1350	-1.21	1.11	0.31	0.72	0.28	8.09E-02
Walcott	8	1361	-0.96	1.63	0.35	0.79	0.21	5.39E-03
Walcott	8	1368.5	8.79	0.80	0.09	0.89	0.11	1.54E-01
Walcott	4	1609	-	1.62	1.27	0.22	0.78	3.12E-03
Walcott	4	1368	13.09	1.21	0.22	0.82	0.18	4.65E-07

Table 2:

depth	[SO ₄] ppm	$\delta^{34}\text{S}_{\text{sulfate}}$	$\delta^{34}\text{S}_{\text{sulfide}}$	$\Delta^{34}\text{S}$
2	-	-	-23.06	-
4.2	113	6.26	-22.06	28.32
185	610	15.05	-4.89	19.94
838	695	16.41	-	-
839	343	20.86	-4.61	25.47
839	342	18.17	-5.41	23.58
883	176	2.10	-2.98	5.08
1146	37	15.88	-	-
1345	77	15.47	-	-
1357	231	8.32	3.00	5.32
1474.5	202	24.57	7.60	16.97
1497.5	136	15.18	13.18	2.00